Drug Delivery Vehicles

Deutsche Ausgabe: DOI: 10.1002/ange.201509507
Internationale Ausgabe: DOI: 10.1002/anie.201509507

Facile Generation of Tumor-pH-Labile Linkage-Bridged Block Copolymers for Chemotherapeutic Delivery

*Chun-Yang Sun[+], Yang Liu[+], Jin-Zhi Du[+], Zhi-Ting Cao, Cong-Fei Xu, and Jun Wang**

Abstract: *Successful bench-to-bedside translation of nanomedicine relies heavily on the development of nanocarriers with superior therapeutic efficacy and high biocompatibility. However, the optimal strategy for improving one aspect often conflicts with the other. Herein, we report a tactic of designing tumor-pH-labile linkage-bridged copolymers of clinically validated poly(D,L-lactide) and poly(ethylene glycol) (PEG-Dlink$_m$-PDLLA) for safe and effective drug delivery. Upon arriving at the tumor site, PEG-Dlink$_m$-PDLLA nanoparticles will lose the PEG layer and increase zeta potential by responding to tumor acidity, which significantly enhances cellular uptake and improves the in vivo tumor inhibition rate to 78.1% in comparison to 47.8% of the non-responsive control. Furthermore, PEG-Dlink$_m$-PDLLA nanoparticles show comparable biocompatibility with the clinically used PEG-b-PDLLA micelle. The improved therapeutic efficacy and safety demonstrate great promise for our strategy in future translational studies.*

Polymeric nanoparticles have received tremendous attention for cancer treatment owing to their improved pharmacokinetics and preferential accumulation at the tumor site by the enhanced permeability and retention (EPR) effect.[1] Although there has been much effort in recent decades, few polymeric formulations have been translated into a clinical setting.[2] While a variety of reasons can be accountable for this predicament, marginal therapeutic effects and potential toxicity are the two typical obstacles.[3]

To improve the therapeutic efficacy, various innovative methods have been reported.[4] One typical approach is to create stimuli-responsive systems with temporal-spatial-controlled drug release or cell interactions.[5] A number of endogenous and exogenous stimuli have been applied to trigger physical or chemical property changes of nanoparticles.[6] Unfortunately, most available stimuli-responsive systems have a limited chance of reaching clinical trial owing to the complexity of architectural design, difficulties in the scaling up, and potential toxicity concerns.[5a] To improve the safety profiles of delivery systems and accelerate clinical translation, clinically validated poly(D,L-lactide) (PDLLA) and poly(ethylene glycol) (PEG) are widely used in the design of delivery carriers.[7] A typical polymeric and nano-therapeutic based on these polymers is Genexol-PM, which is approved in South Korea and is undergoing clinical investigation in the United States.[8] Several other polymeric micelles (NC6004, NK012, and NK105), which are constructed from PEG and polypeptide copolymers, are currently undergoing clinical trials for cancer treatment.[2a,9] Despite marked advances, one potential drawback of these systems is that their in vivo navigation relies solely on a passive targeting effect, which lacks sophisticated features for overcoming the tremendous delivery barriers.[10]

To develop advanced delivery systems with high translational promise, we report a biocompatible and tumor-pH-responsive polymeric nanoparticle based on a bridged PEG and PDLLA block copolymer for improved cancer therapy. The acid-labile copolymer, denoted as PEG-*Dlink$_m$*-PDLLA, was synthesized by covalently connecting PEG and PDLLA segments with an acid-degradable amide bond (Figure 1A; Supporting Information, Scheme S1). This amphiphilic copolymer assembles into PEGylated nanoparticles, which would accumulate preferentially at tumor site. After extravasation into the tumor matrix, the characteristic tumor acidity (pH 6.5–7.0)[11] triggers the cleavage of the amide bond, leading to the release of the PEG corona as well as the increase of zeta potential of the nanoparticle, both of which in turn facilitate cellular uptake (Figure 1B). With loading of docetaxel (DTXL), the enhanced internalization would improve in vitro and in vivo therapeutic efficacy. Moreover, the PEG-*Dlink$_m$*-PDLLA polymer is obtained by minimal modification of clinically validated PEG and PDLLA,[7c] and is expected to show high biocompatibility and safety.

In this study, 2-propionic-3-methylmaleic anhydride (CDM) was first reacted with PEG to obtain PEG-CDM, and its structure was confirmed by ^{1}H and ^{13}C NMR (Supporting Information, Figures S1 and S2). The remaining anhydride group of PEG-CDM was then reacted with 6-amine-1-hexanol to produce PEG-*Dlink$_m$*-OH. The complete reaction was confirmed by the integration ratio between methyl protons of the *Dlink$_m$* moiety and methylene protons of 6-amine-1-hexanol (Figures S3 and S4). Moreover, the splitting of methyl protons in the CDM moiety is attributed to the α and β isomers of the resultant PEG-*Dlink$_m$*-OH, also

[*] C. Sun,[+] Y. Liu,[+] Prof. J. Wang
The CAS Key laboratory of Innate Immunity and Chronic Disease
School of Life Sciences and Medical Center
University of Science and Technology of China
Hefei, 230027 (China)
E-mail: jwang699@ustc.edu.cn
Z. Cao, C. Xu, Prof. J. Wang
Hefei National Laboratory for Physical Sciences at the Microscale
University of Science and Technology of China
Hefei, 230027 (China)
Dr. J. Du[+]
Department of Biomedical Engineering
Emory University and Georgia Institute of Technology
Atlanta, 30322 (USA)
[+] These authors contributed equally to this work.

Supporting information for this article is available on the WWW under http://dx.doi.org/10.1002/anie.201509507.

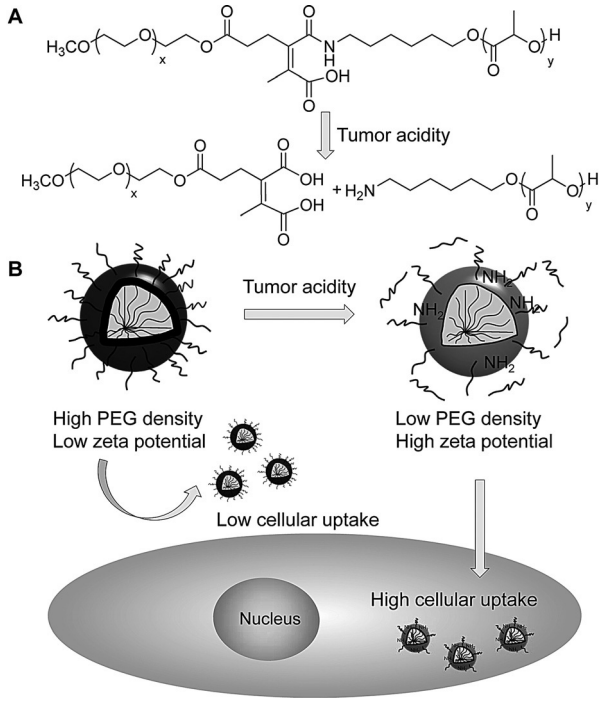

Figure 1. A) Chemical structure of PEG-*Dlink*$_m$-PDLLA and its cleavage under tumor acidity. B) Illustration of enhanced cellular uptake of nanoparticles assembled from PEG-*Dlink*$_m$-PDLLA.

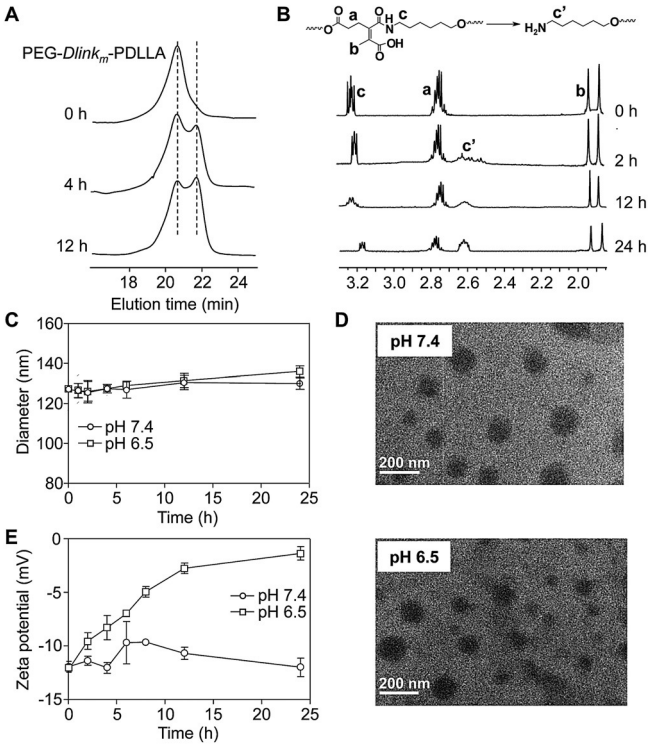

Figure 2. A) GPC profiles of ^{Dlinkm}NP after incubation at pH 6.5 for different periods of time. B) ^{1}H NMR spectra of ^{Dlinkm}NP degradation product after incubation at pH 6.5 for 0, 2, 12, 24 h and the removal of the PEG segment. C) Diameter change of ^{Dlinkm}NP at pH 7.4 or 6.5. D) TEM images of ^{Dlinkm}NP after incubation at pH 7.4 or 6.5 for 12 h. E) Zeta potential change of ^{Dlinkm}NP at pH 7.4 or 6.5.

suggesting successful ring-opening reaction (Figure S3, only the α isomer is depicted for simplicity).[12] PEG-*Dlink*$_m$-OH was employed for the polymerization of D,L-lactide to produce PEG-*Dlink*$_m$-PDLLA copolymer, whose structure and purity were confirmed by gel permeation chromatography (GPC) and NMR analyses (Figures S5–S7). Notably, a series of bridged copolymers with various components and molecular weights could be prepared (Table S1), suggesting the generality of the synthetic route. PEG$_{113}$-*Dlink*$_m$-PDLLA$_{70}$ (the subscript represents degree of polymerization of each block) was chosen for the following studies.

PEG-*Dlink*$_m$-PDLLA self-assembled into nanoparticles (denoted as ^{Dlinkm}NP) in aqueous solution and showed spherical morphology with a diameter of roughly 100 nm (Figure S8). A control polymer PEG-*b*-PDLLA was selected to construct control nanoparticles (denoted as NP) with similar size. Nanoparticles in this size range are believed to be suitable for prolonged circulation and enhanced tumor accumulation through the EPR effect.[13] Furthermore, both ^{Dlinkm}NP and NP showed similar critical micelle concentrations (Figure S9) and encapsulation efficiency of DTXL (ca. 8.0%). At pH 7.4, they showed a similar drug release profile, with approximately 60% drug release after 168 h (Figure S10).

The cleavage of PEG-*Dlink*$_m$-PDLLA was studied at acidic pH. As the GPC profiles show (Figure 2A), a unimodal peak of PEG-*Dlink*$_m$-PDLLA appeared at 20.62 min, while a shoulder at 21.70 min appeared after incubating the ^{Dlinkm}NP at pH 6.5, indicating the scission of the diblock copolymer. The relative intensity of the shoulder gradually increased with extended incubation time. To further verify whether the scission occurs at the acid-labile amide bond, ^{1}H NMR was adopted. ^{1}H NMR spectra in Figure 2B clearly showed that a new peak at 2.63 ppm (peak *c*′), a characteristic resonance of methylene protons adjacent to the amino group, appeared after 2 h incubation. Furthermore, its intensity increased with incubation time, while the intensity of resonance of protons adjacent to the amide bond (peak *c*) decreased concomitantly, strongly suggesting the cleavage of the amide bond. According to the relative integration, nearly 60% of the linker was cleaved after 24 h incubation at pH 6.5. Moreover, the degradation of ^{Dlinkm}NP at pH 7.4 (ca. 15%) and pH 5.5 (ca. 70%) further demonstrate the pH-sensitivity and pH-dependency of the *Dlink*$_m$ moiety (Figure S11).

We then studied the influence of PEG detachment on the size and zeta potential of ^{Dlinkm}NP. ^{Dlinkm}NP was incubated at pH 6.5 or 7.4, and the size and zeta potentials of the particles were monitored. The light scattering results (Figure 2C) indicated that no obvious size change was observed under either pH condition. The transmission electron microscopy (TEM) images also confirmed that ^{Dlinkm}NP was able to keep its original size and shape at both pH values, and no obviously large aggregates were observed (Figure 2D). The zeta potential results indicated that ^{Dlinkm}NP displayed a constantly negative surface charge of around −12 mV at pH 7.4. In contrast, after incubation at pH 6.5, ^{Dlinkm}NP showed a considerable zeta potential increase (Figure 2E). These size and zeta potential changes could be attributed to partial removal

of the PEG corona and the generation of cationic amino groups at the interface after linker cleavage. The ability to prevent particle aggregation, as well as the increase of zeta potential, are expected to be advantageous for facilitating cellular uptake to further contribute to the in vitro and in vivo antitumor efficacy of delivered drugs.

To test our hypothesis, MDA-MB-231 cells were incubated with PCL-Rhodamine B (RhoB)-labeled nanoparticles pre-treated at pH 7.4 or 6.5 for different periods of time. After 2 h of incubation, the intracellular PCL-RhoB was quantified by high performance liquid chromatography (HPLC). As shown in Figure 3A, for the NP group, the

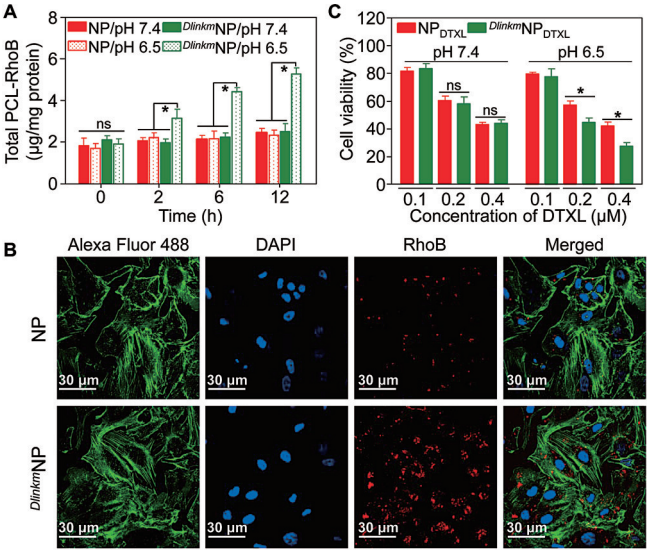

Figure 3. A) Quantitative analysis of cellular uptake of PCL-RhoB-labeled NP and ^{Dlinkm}NP in MDA-MB-231 cells by high performance liquid chromatography. NP or ^{Dlinkm}NP were pre-treated at pH 7.4 or 6.5 for 0, 2, 6, and 12 h, then incubated with cells for 2 h. B) Confocal images of cellular uptake of PCL-RhoB-labeled NP and ^{Dlinkm}NP. The nanoparticles were pre-treated at pH 6.5 for 6 h, then incubated with cells for 2 h. Cell nuclei and β-actin are stained with 4′,6-diamidino-2-phenylindole (DAPI, blue) and Alexa Fluor 488 (green), respectively. C) Cytotoxicity of $^{Dlinkm}NP_{DTXL}$ and NP_{DTXL} against MDA-MB-231 cells. The cells were incubated with nanoparticles for 12 h at pH 7.4 or 6.5, then further incubated with fresh medium for 36 h. $^*p < 0.05$. ns = no significant difference.

internalized amount of PCL-RhoB was almost constant, regardless of the pre-treated pH and time. For the ^{Dlinkm}NP group pre-treated at pH 7.4, the uptake was comparable to that of the NP group. However, the ^{Dlinkm}NP group pre-treated at pH 6.5 showed clear time-dependent internalization patterns. Significantly enhanced intracellular PCL-RhoB content was observed with pre-treatment time increasing from 0 h to 12 h ($p < 0.05$), suggesting efficient internalization of micelles after PEG detachment and zeta potential increase. The confocal images also visually substantiated our statement by showing that more punctate red fluorescence was observed in the cells receiving ^{Dlinkm}NP treatment (Figure 3B). Previous reports have also observed that PEG deshielding enables to facilitation of cellular uptake.[14]

The cell-killing efficacy was evaluated at varying DTXL concentrations using the 3-(4,5-dimethylthiazol-2-yl)-2,5-diphenyl tetrazolium bromide (MTT) assay (Figure 3C). At pH 7.4, both $^{Dlinkm}NP_{DTXL}$ and NP_{DTXL} showed comparable cell growth inhibition with increasing DTXL concentration. However, when they were incubated at pH 6.5, $^{Dlinkm}NP_{DTXL}$ and NP_{DTXL} showed different cytotoxicities. Significantly enhanced cell-killing efficacy was observed with $^{Dlinkm}NP_{DTXL}$ treatment, especially when the DTXL concentrations were 0.2 and 0.4 μM ($p < 0.05$). This result is consistent with the internalization observations, indicating that improved cell-killing can be a result of the enhanced cellular internalization of $^{Dlinkm}NP_{DTXL}$ at pH 6.5.

Next, we studied the in vivo performance of ^{Dlinkm}NP as the drug carrier. Results shown in Figure 4A reveal that both

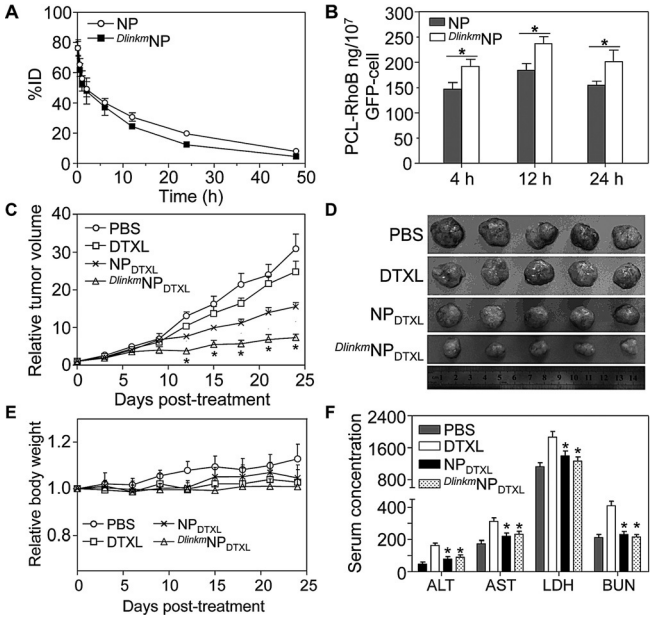

Figure 4. A) Pharmacokinetics of PCL-RhoB-labeled nanoparticles after intravenous administration (mean ± SD, $n = 4$). B) Content of PCL-RhoB in GFP-expressing MDA-MB-231 cells after administration (mean ± SD, $n = 4$), $^*p < 0.05$. C) Tumor growth inhibition of MDA-MB-231 tumor xenograft with different formulations. The injections were performed on days 0, 7, 14, and 21 with an equivalent DTXL dose of 3.5 mg kg^{-1} (mean ± SD, $n = 5$). $^*p < 0.05$, versus NP_{DTXL}. D) Images of MDA-MB-231 xenograft tumor mass excised after the treatment. E) Body weight monitoring of the mice receiving different treatments. F) Enzyme-linked immunosorbent examination of mouse alanine aminotransferase (ALT, U L^{-1}), aspartate transaminase (AST, U L^{-1}), lactate dehydrogenase (LDH, U L^{-1}), blood urea nitrogen (BUN, 10 μmol L^{-1}) in the serum after receiving injection of DTXL or DTXL-loaded nanoparticles. $^*p < 0.05$, versus DTXL.

^{Dlinkm}NP ($t_{1/2z} = 10.48$ h) and NP ($t_{1/2z} = 11.14$ h) showed long blood circulation time, which gives the nanoparticles more opportunity to extravasate from the tumor vessels.[15] Quantitative analysis of PCL-RhoB in homogenized organs showed that both NP and ^{Dlinkm}NP were inevitably captured by liver and spleen (Figure S12), which is a common feature for nanoscale delivery systems.[16] On the other hand, it was found that ^{Dlinkm}NP showed significantly higher tumor enrichment at

12 and 24 h in comparison to the insensitive NP treatment (Figure S13, $p < 0.05$). Moreover, green fluorescent protein (GFP)-expressing MDA-MB-231 tumor xenografts were established to test if the nanoparticles were captured by cancer cells. As shown in Figure 4B, the ^{Dlinkm}NP treatment showed significantly enhanced internalization and retention compared with NP group at each time point. Considering that both ^{Dlinkm}NP and NP have similar size, surface charge, and pharmacokinetics, the improved tumor retention and tumor cell internalization can be a result of the increased cell–nanoparticle interaction, resulting from the tumor-acidity-activated polymer cleavage.

The in vivo tumoricidal effect of $^{Dlinkm}NP_{DTXL}$ was examined in an MDA-MB−231 xenograft tumor model. As shown in Figure 4C, compared with the phosphate-buffered saline (PBS) control, free DTXL showed minimal inhibition of tumor growth with a tumor inhibition rate (TIR) of 16.8%. NP_{DTXL} treatment showed a moderate antitumor effect with a TIR of 47.8%. In contrast, $^{Dlinkm}NP_{DTXL}$ exhibited significantly improved antitumor efficacy, with a TIR of 78.1% ($p < 0.05$, versus the NP_{DTXL} group). Moreover, the significant inhibition could be observed from day 12 post-treatment, by which time only two doses had been injected, indicating the high effectiveness of the $^{Dlinkm}NP_{DTXL}$ treatment. The images (Figure 4D) and weights (Figure S14) of tumor mass excised after the treatment further confirmed the superior antitumor activity of $^{Dlinkm}NP_{DTXL}$. Meanwhile, no body weight loss was observed during the therapeutic period (Figure 4E). Histological examination and immunohistochemistry of the tumor sections demonstrated that extensive regions of apoptotic and non-proliferative cells were present in mice receiving $^{Dlinkm}NP_{DTXL}$ (Figure S15).

In vivo toxicity of nanoparticles is another crucial parameter for preclinical evaluation.[17] As mentioned, PEG-*Dlink*$_m$-PDLLA was synthesized from minimal modification of the clinically validated PEG and PDLLA polymers, and is anticipated to show good biocompatibility. To verify it, various tests associated with material safety profiles were conducted. After receiving systemic injection of NP or ^{Dlinkm}NP at polymer doses as high as 2 g kg^{-1}, all of the mice were alive after 21 days. Hematological analysis showed all the studied parameters after injection were normal, except that the white blood cell counts was increased, likely attributed to the inflammation in the lymph nodes induced by nanoparticles entering into lymphatic system after intravenous injection (Figure S16). The analysis of alanine aminotransferase, aspartate aminotransferase, lactate dehydrogenase, and blood urea nitrogen (Figure S17) indicated that both ^{Dlinkm}NP and NP had minimum effects on liver and kidney function, suggesting the *Dlink*$_m$ bridged copolymer was compatible for in vivo drug delivery. On the other hand, following the drug encapsulation, $^{Dlinkm}NP_{DTXL}$ and NP_{DTXL} exhibited much higher LD_{50} in acute toxicity studies compared with DTXL, demonstrating the formulations were well tolerated by mice (Table S2). Noticeable organ damage was further observed in the DTXL group by histological analysis and liver and kidney function assays (Figure 4F; Supporting Information, Figure S18). Altogether, the toxicity studies confirmed that ^{Dlinkm}NP is biocompatible and has potential for drug delivery.

In conclusion, we have successfully constructed a tumor-acidity-responsive nanoparticle through designing bridged PEG and PDLLA copolymers with an acid-labile linker. As a result of the tumor-acid-activated PEG detachment and increased surface charge, enhanced cellular uptake, and improved in vitro and in vivo antitumor activities were achieved in comparison with PEG-*b*-PDLLA. Moreover, the new polymer shows an excellent safety profile comparable to the pharmaceutically approved PEG-*b*-PDLLA. Besides introducing a covalent bond to construct bridged copolymers, designing copolymers containing ionizable hydrophobic blocks allows controllable and much sharper pH responses at the millisecond timescale.[5b,11b,18] In comparison with those ultra-pH-sensitive materials, slower degradation of the bridged *Dlink*$_m$ moiety, which take time to respond to external stimuli, may partially limit the therapeutic efficacy. More advanced linkages are necessary in future studies. Although the responsiveness should be improved, our research presents a tactic to chemically modify clinically validated PEG-*b*-PDLLA. Considering the facile synthetic route, as well as the nanoparticle preparation, this is promising for the development of a robust and scalable process to prepare ^{Dlinkm}NP for potential translational studies in the future.

Acknowledgements

This work was supported by the National Basic Research Program of China (2015CB932100, 2013CB933900, 2012CB932500), and the National Natural Science Foundation of China (51125012, 51390482).

Keywords: bridged copolymers · clinical translation · drug delivery · nanoparticles · tumor-acidity-responsive

How to cite: *Angew. Chem. Int. Ed.* **2016**, *55*, 1010–1014
Angew. Chem. **2016**, *128*, 1022–1026

[1] a) K. Kataoka, A. Harada, Y. Nagasaki, *Adv. Drug Delivery Rev.* **2001**, *47*, 113; b) Y. Matsumura, H. Maeda, *Cancer Res.* **1986**, *46*, 6387.

[2] a) H. Cabral, K. Kataoka, *J. Controlled Release* **2014**, *190*, 465; b) V. J. Venditto, F. C. Szoka, *Adv. Drug Delivery Rev.* **2013**, *65*, 80; c) D. L. Stirland, J. W. Nichols, S. Miura, Y. H. Bae, *J. Controlled Release* **2013**, *172*, 1045.

[3] a) K. Riehemann, S. W. Schneider, T. A. Luger, B. Godin, M. Ferrari, H. Fuchs, *Angew. Chem. Int. Ed.* **2009**, *48*, 872; *Angew. Chem.* **2009**, *121*, 886; b) W. R. Sanhai, J. H. Sakamoto, R. Canady, M. Ferrari, *Nat. Nanotechnol.* **2008**, *3*, 242; c) H. Y. Xue, S. Liu, H. L. Wong, *Nanomedicine* **2014**, *9*, 295.

[4] a) T. M. Sun, Y. S. Zhang, B. Pang, D. C. Hyun, M. X. Yang, Y. N. Xia, *Angew. Chem. Int. Ed.* **2014**, *53*, 12320; *Angew. Chem.* **2014**, *126*, 12520; b) Z. L. Cheng, A. Zaki, J. Z. Hui, V. R. Muzykantov, A. Tsourkas, *Science* **2012**, *338*, 903.

[5] a) S. Mura, J. Nicolas, P. Couvreur, *Nat. Mater.* **2013**, *12*, 991; b) E. S. Lee, Z. G. Gao, Y. H. Bae, *J. Controlled Release* **2008**, *132*, 164; c) Z. S. Ge, S. Y. Liu, *Chem. Soc. Rev.* **2013**, *42*, 7289.

[6] a) R. Tong, L. Tang, L. Ma, C. L. Tu, R. Baumgartner, J. J. Cheng, *Chem. Soc. Rev.* **2014**, *43*, 6982; b) Q. Zhang, N. R. Ko, J. K. Oh, *Chem. Commun.* **2012**, *48*, 7542; c) T. Mizuhara, K. Saha, D. F. Moyano, C. S. Kim, B. Yan, Y. K. Kim, V. M. Rotello, *Angew. Chem. Int. Ed.* **2015**, *54*, 6567 – 6570; *Angew. Chem.* **2015**, *127*, 6667 – 6670.
[7] a) J. Hrkach, et al., *Sci. Transl. Med.* **2012**, *4*, 128ra139; b) K. Knop, R. Hoogenboom, D. Fischer, U. S. Schubert, *Angew. Chem. Int. Ed.* **2010**, *49*, 6288; *Angew. Chem.* **2010**, *122*, 6430; c) K. Avgoustakis, *Curr. Drug Delivery* **2004**, *1*, 321.
[8] H. K. Ahn, M. Jung, S. J. Sym, D. B. Shin, S. M. Kang, S. Y. Kyung, J.-W. Park, S. H. Jeong, E. K. Cho, *Cancer Chemother. Pharmacol.* **2014**, *74*, 277.
[9] Y. Z. Min, J. M. Caster, M. J. Eblan, A. Z. Wang, *Chem. Rev.* **2015**, *115*, 11147.
[10] a) V. P. Chauhan, R. K. Jain, *Nat. Mater.* **2013**, *12*, 958; b) E. Blanco, H. Shen, M. Ferrari, *Nat. Biotechnol.* **2015**, *33*, 941.
[11] a) M. G. Vander Heiden, L. C. Cantley, C. B. Thompson, *Science* **2009**, *324*, 1029; b) Y. G. Wang, K. J. Zhou, G. Huang, C. Hensley, X. N. Huang, X. P. Ma, T. Zhao, B. D. Sumer, R. J. DeBerardinis, J. M. Gao, *Nat. Mater.* **2014**, *13*, 204; c) K. Maier, E. Wagner, *J. Am. Chem. Soc.* **2012**, *134*, 10169.
[12] H. Takemoto, K. Miyata, S. Hattori, T. Ishii, T. Suma, S. Uchida, N. Nishiyama, K. Kataoka, *Angew. Chem. Int. Ed.* **2013**, *52*, 6218; *Angew. Chem.* **2013**, *125*, 6338.
[13] J. Q. Wang, W. W. Mao, L. L. Lock, J. B. Tang, M. H. Sui, W. L. Sun, H. G. Cui, D. Xu, Y. Q. Shen, *ACS Nano* **2015**, *9*, 7195.
[14] a) F. Perche, S. Biswas, T. Wang, L. Zhu, V. P. Torchilin, *Angew. Chem. Int. Ed.* **2014**, *53*, 3362; *Angew. Chem.* **2014**, *126*, 3430; b) X. Z. Yang, J. Z. Du, S. Dou, C. Q. Mao, H. Y. Long, J. Wang, *ACS Nano* **2012**, *6*, 771.
[15] a) K. Cho, X. Wang, S. M. Nie, Z. Chen, D. M. Shin, *Clin. Cancer Res.* **2008**, *14*, 1310; b) R. Mo, T. Y. Jiang, Z. Gu, *Angew. Chem. Int. Ed.* **2014**, *53*, 5815; *Angew. Chem.* **2014**, *126*, 5925.
[16] G. S. Kwon, M. Yokoyama, T. Okano, Y. Sakurai, K. Kataoka, *Pharm. Res.* **1993**, *10*, 970.
[17] L. Yildirimer, N. T. K. Thanh, M. Loizidou, A. M. Seifalian, *Nano Today* **2011**, *6*, 585.
[18] a) K. J. Zhou, Y. G. Wang, X. N. Huang, K. Ludy-Phelps, B. D. Sumer, J. M. Gao, *Angew. Chem. Int. Ed.* **2011**, *50*, 6109; *Angew. Chem.* **2011**, *123*, 6233; b) X. P. Ma, Y. G. Wang, T. Zhao, Y. Li, L.-C. Su, Z. H. Wang, G. Huang, B. D. Sumer, J. M. Gao, *J. Am. Chem. Soc.* **2014**, *136*, 11085; c) C. S. Wang, et al., *Nat. Commun.* **2015**, *6*, 8524.

Received: October 11, 2015
Revised: November 10, 2015
Published online: December 3, 2015

